Clay Minerals (2022), **57**, 105–113
doi:10.1180/clm.2022.26

CAMBRIDGE UNIVERSITY PRESS

Article

Sorption of Congo Red anionic dye on natural hydrotalcite and stichtite: kinetics and equilibrium

Olga V. Nestroinaia, Irina G. Ryltsova, Maksim N. Yaprintsev, Evgeniya Yu. Nakisko, Evgeniy S. Seliverstov and Olga E. Lebedeva*

Belgorod State National Research University, Belgorod, 308015, Russia

Abstract

The sorption properties of two layered minerals of the hydrotalcite supergroup – hydrotalcite and stichtite – were investigated with the aim of determining their kinetic parameters of sorption and their adsorption isotherm type. Pristine hydrotalcite and stichtite were characterized using X-ray diffraction, Fourier-transform infrared spectroscopy, scanning electron microscopy, energy-dispersive X-ray analysis and laser diffraction analysis of the particle-size distribution. The 'memory effect' of the sorbents was examined after calcination at 650°C. Slight indications of reconstructed hydrotalcite were observed, while the stichtite dehydration–rehydration cycle was irreversible. The hydrotalcite and stichtite were used to remove Congo Red from the aqueous solution. The pseudo-second order kinetic model described the process adequately. Mixed external and internal diffusion was confirmed for both minerals. The sorption of Congo Red on stichtite fits the Langmuir model. Stichtite demonstrated a maximum adsorption capacity of 2.5 mmol g^{-1} at 35°C. Increasing temperature increased the adsorption rate of Congo Red on stichtite but did not affect the adsorption rate constant for hydrotalcite.

Keywords: Congo Red, hydrotalcite, natural layered double hydroxides, stichtite, sorption isotherms, sorption kinetics

(Received 18 December 2021; revised 17 September 2022; Accepted Manuscript online: 6 October 2022; Associate Editor: M. Pospíšil)

The hydrotalcite supergroup combines natural layered double hydroxides (LDH), characterized by a brucite-like structure of positively charged metal hydroxide layers with interlayer anions and various numbers of water molecules. The first phase of the LDH structure is hydrotalcite, a double hydroxide of magnesium and aluminium with a carbonate anion in the interlayer space, which gives its name to this supergroup of minerals (Mills *et al.*, 2011, 2012). Other members of the hydrotalcite minerals supergroup can contain not only carbonate anions, but also sulfate or chloride ions (the latter being rarer). The cationic composition of natural LDHs is also quite variable: copper, nickel, iron (II and III), zinc, chromium, manganese, sodium and strontium cations can be located in the brucite-like layer. The presence of anions in the interlayer spaces of these minerals gives rise to another common name for this group of compounds: anionic clays.

The LDHs are of interest because of their possible use as catalysts and photocatalysts (Wei *et al.*, 2008; Mantilla *et al.*, 2009; Tanasoi *et al.*, 2011; Fan *et al.*, 2014; Liu *et al.*, 2020), precursors of catalysts (Daza *et al.*, 2010; Damindarova *et al.*, 2020), ion exchangers (Chubar *et al.*, 2017), drug-delivery systems (Wang *et al.*, 2005; Rives *et al.*, 2014, Lopez *et al.*, 2019), among other applications. The effectiveness of the application of LDHs as sorbents is recognized widely, and numerous examples have been published (e.g. Tezuka *et al.*, 2005; Goha *et al.*, 2008; Liang *et al.*, 2013). It is noteworthy that a substantial number of publications, including those mentioned above, are devoted to the study of the properties of synthetic LDHs. Papers concerning natural LDHs are rather uncommon (Frost & Erickson, 2004; Correcher & Garcia-Guinea, 2018; Turvey *et al.*, 2018). Krivovichev *et al.* (2012) and Zhitova *et al.* (2018) provide detailed descriptions of the mineralogies of a variety of representatives of the hydrotalcite supergroup. Stichtite was described in the comprehensive review by Theiss *et al.* (2013). Using natural minerals for the removal of water pollutants is very attractive as the structure of the minerals of the hydrotalcite supergroup makes them the only natural anion exchangers (de Castro *et al.*, 2018). However, to the best of our knowledge, there have been no publications on the physicochemical parameters of adsorption on natural LDHs of the hydrotalcite supergroup; namely, their kinetic and equilibrium characteristics and regime discriminations have not been determined. Data for these parameters would allow us to describe, preview and regulate such sorption processes.

The present study focuses on two natural LDHs – hydrotalcite and stichtite – and on their sorption properties towards Congo Red dye as a common model anionic dye in sorption investigations. The aim of the research was to determine the kinetic parameters of the sorption process and to describe the adsorption isotherms.

*Email: olebedeva@bsu.edu.ru

Cite this article: Nestroinaia OV, Ryltsova IG, Yaprintsev MN, Nakisko EYu, Seliverstov ES, Lebedeva OE (2022). Sorption of Congo Red anionic dye on natural hydrotalcite and stichtite: kinetics and equilibrium. *Clay Minerals* **57**, 105–113. https://doi.org/10.1180/clm.2022.26

Materials

Natural hydrotalcite ($Mg_6Al_2(CO_3)(OH)_{16}{\cdot}4H_2O$, hereinafter designated as MgAl-LDH) from Praskovie-Evgenievskaya Mine

(Chelyabinsk region, Southern Urals) and stichtite (MgCr-LDH) from the Terektinsky ridge (Ust-Koksinsky district, Altai Republic, southern Siberia) were used in the study. Stichtite is a magnesium–chromium hydroxycarbonate mineral with the general formula $Mg_6Cr_2(OH)_{16}CO_3{\cdot}H_2O$. The Cr^{3+} ion can be substituted isomorphically by Fe^{3+}, so trivalent iron is common in stichtite (Mills *et al.*, 2011; Miandad *et al.*, 2018). Prior to the characterization and sorption experiments, the samples were ground in a ball mill and then in a mortar.

Congo Red ($C_{32}H_{22}N_6Na_2O_6S_2$, disodium salt of 4,4'-bis-(1-amino-4-sulfo-2-naphthylazo) biphenyl) is a synthetic heterocyclic aromatic azo dye. 'Analytically pure' Congo Red dye was used without additional purification in this work. This azo dye is a common model sorbate that is often used in studies of the sorption properties of LDHs and their thermal degradation products (Li *et al.*, 2016; Miandad *et al.*, 2018; Zhang *et al.*, 2018; Chilukoti & Thangavel, 2019).

Experimental

X-ray diffraction (XRD) phase analysis was carried out using a Rigaku diffractometer with Cu-*K*α radiation (λ =1.5406 Å) with a scanning step of 0.02°2θ in the range 5–75°2θ. The analysis was performed using the Debye–Scherrer–Hell powder method. Sample preparation was carried out by grinding the LDH samples in an agate mortar to a fine powder. XRD traces were analysed with reference to the ICDD PDF2 internal database. The lattice parameters of the natural hydrotalcites were calculated using Rietveld refinement.

The particle-size distribution of the LDH samples was determined in suspension using a Microtrac S3500 laser particle size analyser. The measurement range of particle sizes in the suspension was 0.02–2800 μm. The samples were immersed in an analyser cell filled with distilled water, then dispersed by ultrasound for 60 s. Particle size was determined in three dimensions. The relative measurement error in this range is ±10.0% at $p = 0.95$.

The morphological characteristics of the LDH particles were determined using scanning electron microscopy (SEM; Hitachi SU1510). The crushed, finely dispersed samples were placed on a carbon film support. The images were acquired at an accelerating voltage of 30 kV in a high vacuum using a backscattered electron detector.

The contents of metal cations in the samples were determined using an FEI Quanta 200 3D SEM equipped with an energy-dispersive X-ray analysis (EDX) system at an operating voltage of 30 kV.

Fourier-transform infrared (FTIR) spectra were recorded from 400 to 4000 cm^{-1} using a Shimadzu IR Prestige 21 spectrometer. The spectra were recorded at room temperature in samples diluted with potassium bromide at a 1:50 mass ratio.

To study the behaviour in the dehydration–rehydration cycle (the 'memory effect'; Cavani *et al.*, 1991; Evans & Slade, 2006), the natural LDHs were calcined in air at 650°C for 120 min at a heating rate of 20°C min^{-1} in a MIMP Tulacika-17 muffle furnace. The calcined samples were rehydrated in an aqueous medium with constant stirring for 24 h. The rehydrated samples were dried at 110–120°C.

The adsorption experiments were carried out to estimate the effects of initial Congo Red concentration, contact time and temperature on the adsorption of Congo Red on natural LDHs. The adsorption experiments were performed at 25°C and 35°C. A TC-1/20CPU electric dry-air thermostat was used to maintain a constant temperature. In a typical experiment, 25 mL of Congo Red aqueous solution was added to 0.1 g of natural LDH and left in the thermostat for a predetermined time interval in the case of the kinetic experiments or until achieving sorption equilibrium in the system in the case of the equilibrium experiments (on the effect of initial Congo Red concentration). Then, the suspension was centrifuged for 10 min at 3000 rpm. The dye concentration in the solution was determined spectrophotometrically using a Specord 210 PLUS Analytik Jena spectrophotometer. The optical densities of the solutions were recorded at a wavelength of 500 nm in a 10 mm cuvette using distilled water as a blank solution.

The Congo Red uptake by the sorbent was calculated using Equation 1:

$$q_t = \frac{(C_0 - C_t)V}{m} \tag{1}$$

where m (g) is the amount of sorbent used, V (L) is the volume of the solution, C_0 and C_t are the initial and final Congo Red concentrations of the solution (mmol L^{-1}) and q_t (mmol g^{-1}) is the amount of Congo Red adsorbed on the solid.

The following kinetic models were applied to fit the experimental data: the Lagergren pseudo-first order model (Equation 2; Lagergren 1898), the pseudo-second order model (Equation 3; Ho & McKay, 1999), the Weber intraparticle diffusion model (Equation 4; Weber & Morris, 1963) and the film diffusion model (Equation 5; Boid *et al.*, 1949):

$$\ln(q_e - q_t) = \ln(q_e) - k_1 t \tag{2}$$

$$\frac{t}{q_t} = \frac{1}{k_2 q_e^2} + \frac{1}{q_e} t \tag{3}$$

$$q_t = k t^{0.5} + C \tag{4}$$

$$\ln(1 - F) = -rt \tag{5}$$

where q_e and q_t are the amounts of Congo Red dye adsorbed (mmol g^{-1}) at equilibrium and at time t (min), respectively; k_1 (min^{-1}) and k_2 (g $mmol^{-1}$ min^{-1}) are the pseudo-first order and pseudo-second order rate constants, respectively; k is the intraparticle diffusion rate constant and C is the intercept; and r is the rate constant for film diffusion (min^{-1}) and F is the fractional attainment.

Two different sorption isotherms equations – the Langmuir equation (Equation 6) and the Freundlich equation (Equation 7) – were used for fitting the experimental data:

$$\frac{1}{q_e} = \frac{1}{q_m} + \frac{1}{K_L q_m C} \tag{6}$$

$$\ln q_e = \ln K_F + \frac{1}{n} \ln C_e \tag{7}$$

where q_e is the amount of Congo Red dye adsorbed (mmol g^{-1}) at equilibrium, C_e is the concentration of solute in the solution at equilibrium, q_m is the maximum loading capacity, K_L is Langmuir equation constant and K_F and 1/n are the Freundlich equation constants.

https://doi.org/10.1180/clm.2022.26 Published online by Cambridge University Press

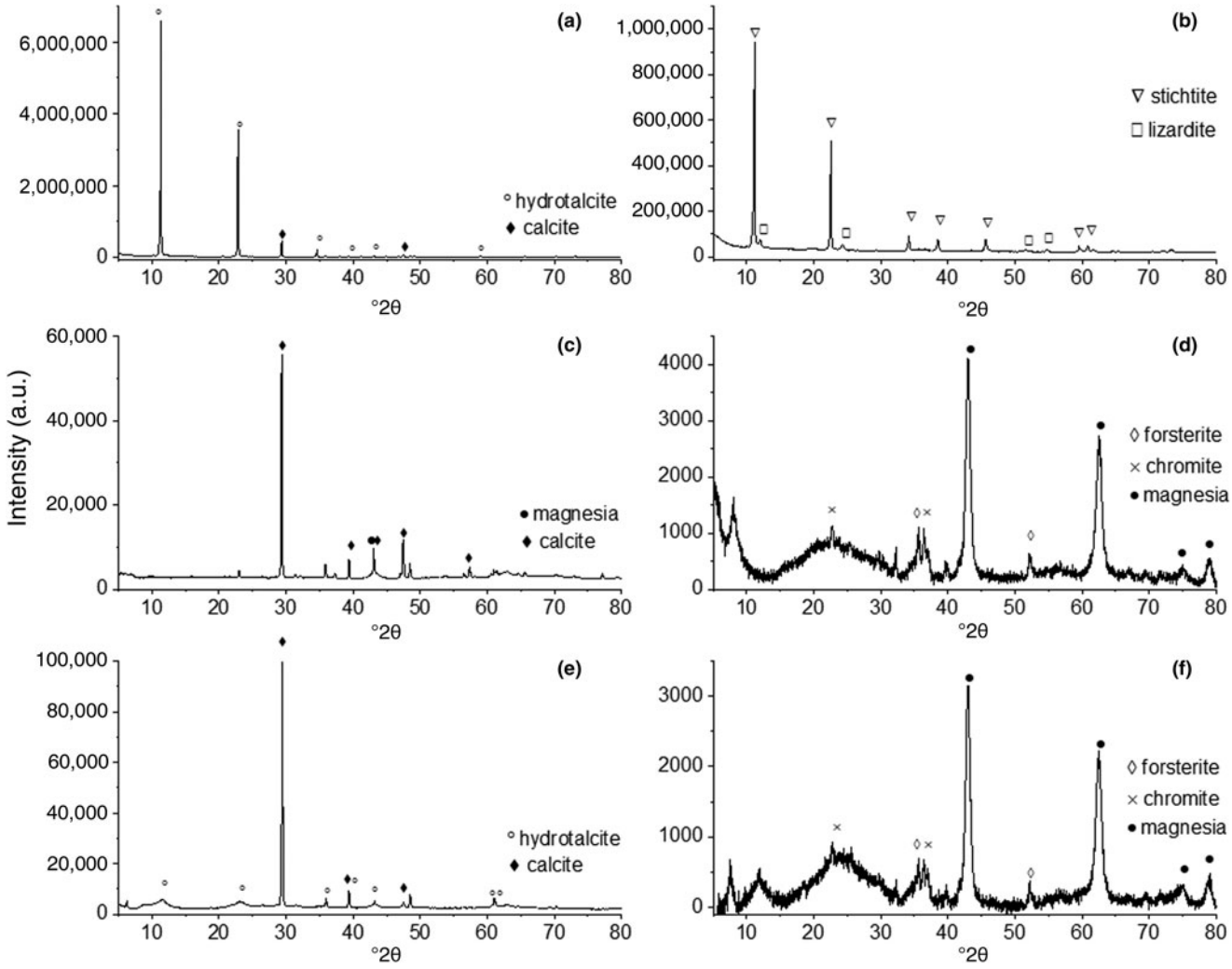

Fig. 1. XRD traces of the LDHs. Original: (a) MgAl-LDH, (b) MgCr-LDH; after calcination at 650°C: (c) MgAl-LDH, (d) MgCr-LDH; after a cycle of dehydration–rehydration: (e) MgAl-LDH, (f) MgCr-LDH.

Results and discussion

Characterization of the mineral samples

The XRD traces of the samples are shown in Fig. 1. The traces are typical for this class of LDHs. In the XRD trace of the MgAl-LDH, the entire set of characteristic reflections corresponding to the (003), (006) and (009/012) basal reflections, and the (015), (018), (110) and (113) reflections are also present (card number 00-014-0191; Cavani *et al.*, 1991; Evans & Slade, 2006). The first peaks for both samples are narrow and intense. This often indicates a high degree of crystal order of the minerals. In addition to characteristic peaks, there are also peaks belonging to impurities. Thus, the hydrotalcite sample contains <5 wt.% calcite ($CaCO_3$, card number 01-081-2027). In the XRD trace of stichtite, trace hydrotalcite was also detected (card number 00-045-1475), and lizardite ($Mg_3Si_2O_5(OH)_4$, card number 01-089-6275, <6 wt.%) was also present.

The parameters *a* and *c* are the parameters for a hexagonal unit cell. They were calculated using Rietveld refinement (Table 1). Hydrotalcite is known to exhibit two polytypes, namely 3R (rhombohedral phase) and 2H, which is also called manasseite (hexagonal phase; Mills *et al.* 2012). According to the results obtained, both the hydrotalcite and the stichtite used in the present study belong to the 3R polytype.

The particle-size distribution was heterogenous and relatively wide (Fig. 2). The average particle sizes for MgAl-LDH and for MgCr-LDH were 71 and 34 μm, respectively.

The layered structure and hexagonal shape of the particles, which are typical for LDHs, were distinguishable in the SEM images. The particle size found using SEM varied from 10 to 70 μm (Fig. 3), which matches the results from the granulometric analysis.

As expected, chemical elements associated with impurities were detected in the compositions of the LDH samples studied. Abundant Ca was detected in hydrotalcite and Si was observed

Table 1. Elemental composition and crystal lattice parameters of the hydrotalcite and stichtite phases.

Sample	Elemental composition (atomic %)								*a* (Å)	*c* (Å)
	Mg	Ca	Cr	Al	Si	Fe	O	N		
MgAl-LDH	13.01	12.24	0.10	4.33	0.45	0.14	57.86	11.87	3.08	23.35
MgCr-LDH	31.61	–	4.86	1.15	6.36	3.11	52.88	–	3.01	23.67

https://doi.org/10.1180/clm.2022.26 Published online by Cambridge University Press

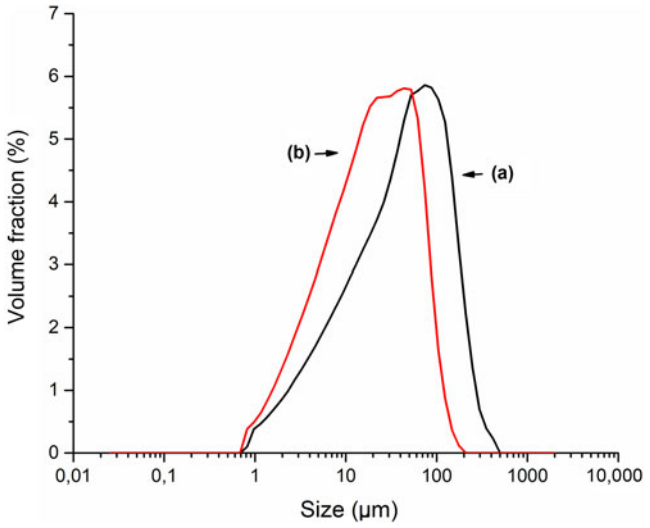

Fig. 2. The distribution of particle sizes of the LDHs: (a) MgAl-LDH, (b) MgCr-LDH.

in stichtite (Fig. 4). This is in accordance with the XRD data, which demonstrated the presence of calcite and lizardite. Table 1 presents the contents of all such chemical elements. The carbon signal was subtracted from the EDX spectra because its amount cannot be determined reliably due to the use of carbon tape for fixing the samples.

The FTIR spectra contain most of the representative bands of LDHs (Fig. 5). The broad intense band with the maximum in the range of 3450–3600 cm^{-1} corresponds to vibrations of OH^- in metal hydroxide layers and interlayer water molecules, and a weak shoulder at 3000–3350 cm^{-1} is due to vibrations of hydroxyl groups of water molecules connected by hydrogen bonds with carbonate anions. The bending mode of the interlayer water can be observed at ~1640 cm^{-1}. The split band of low intensity at 2295–2375 cm^{-1} often refers to atmospheric CO_2. The spectra show a wide band at 1325–1500 cm^{-1} with maxima at 1417 cm^{-1} (MgAl-LDH) and 1386 cm^{-1} (MgCr-LDH) associated with asymmetric stretching vibrations of carbonate ions in the interlayer space of the hydrotalcite-like phase and calcite phase in the case of the MgAl-LDH sample. In addition, bands associated

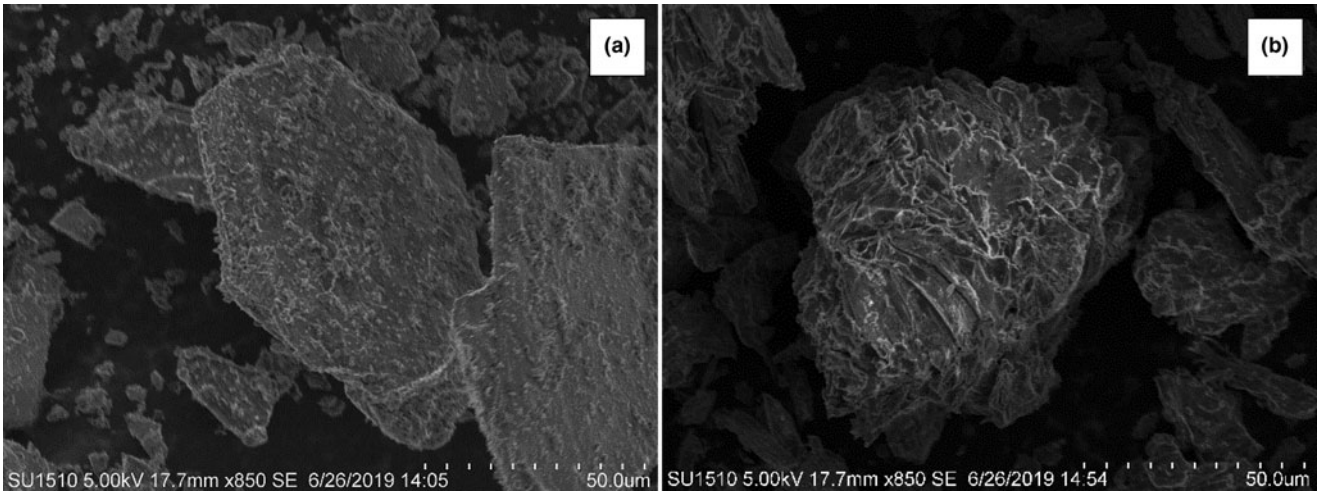

Fig. 3. SEM images of LDH samples: (a) MgAl-LDH, (b) MgCr-LDH.

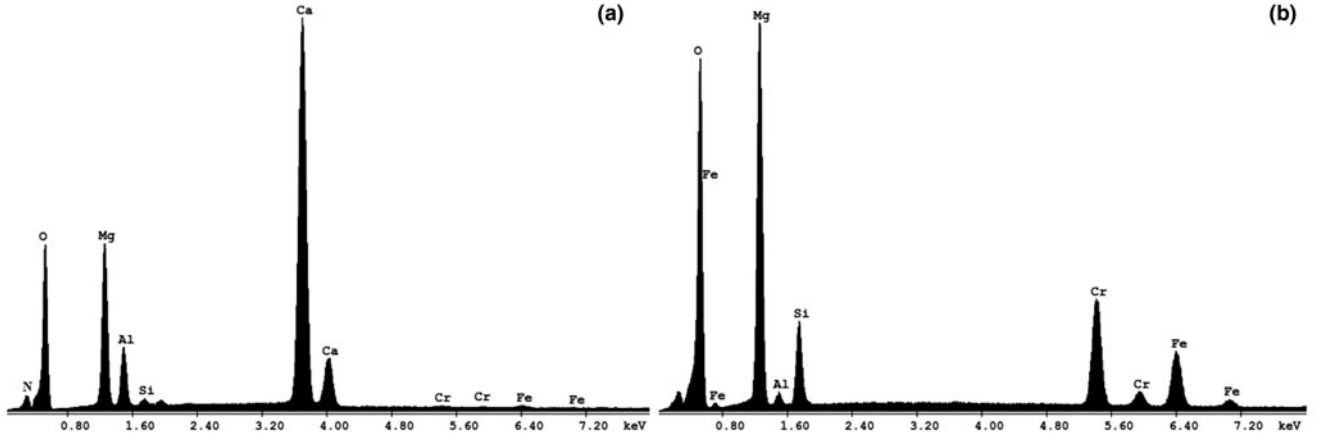

Fig. 4. EDX spectra of the LDH samples: (a) MgAl-LDH, (b) MgCr-LDH.

https://doi.org/10.1180/clm.2022.26 Published online by Cambridge University Press

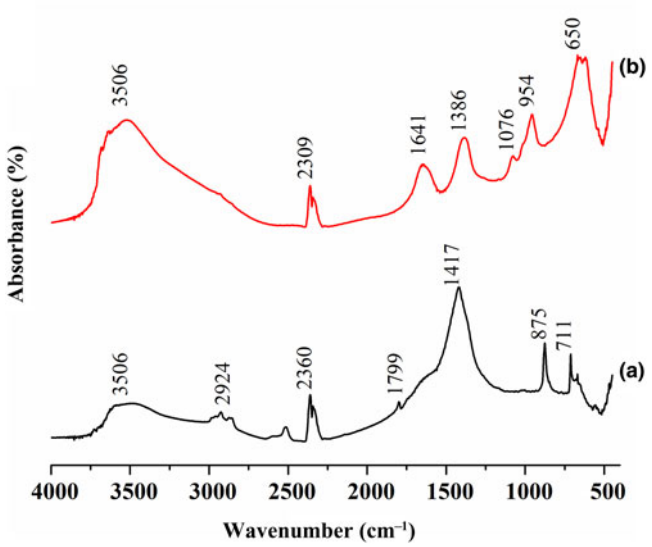

Fig. 5. FTIR spectra of the LDH samples: (a) MgAl-LDH, (b) MgCr-LDH.

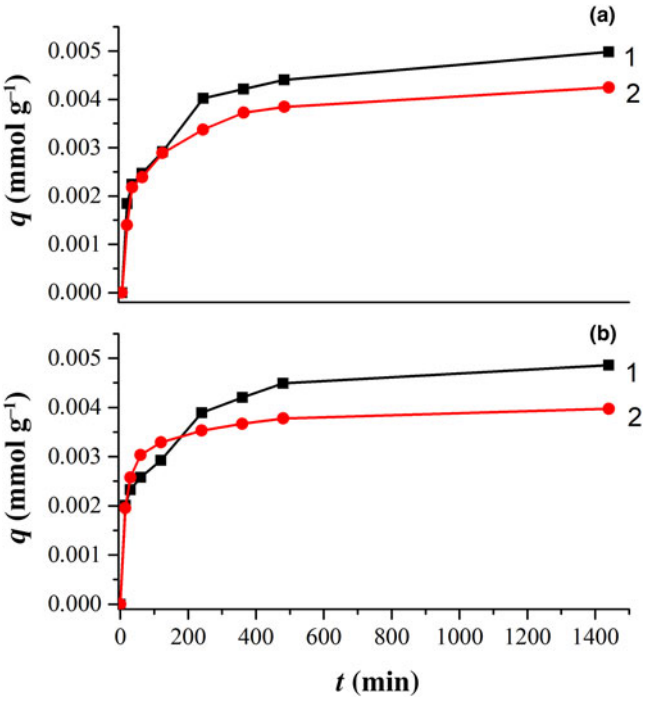

Fig. 6. Kinetic curves of Congo Red sorption on natural LDHs in aqueous solution: (a) at 25°C: 1 = MgAl-LDH, 2 = MgCr-LDH; (b) at 35°C: 1 = MgAl-LDH, 2 = MgCr-LDH.

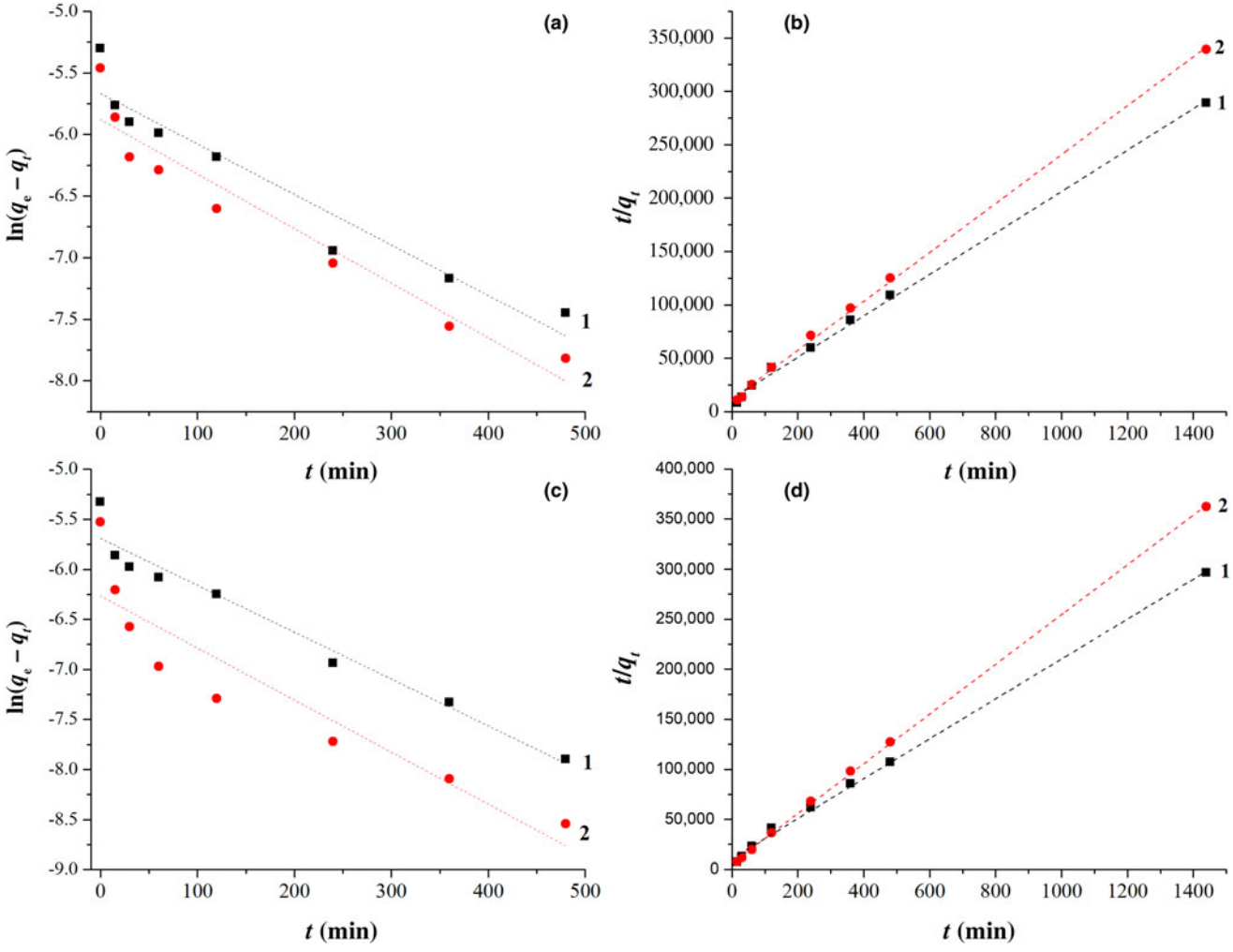

Fig. 7. Application of (a) the pseudo-first order model and (c) the pseudo-second order model for the adsorption of Congo Red at 25°C. Application of (b) the pseudo-first order model and (d) the pseudo-second order model for adsorption of Congo Red at 35°C. 1 = MgAl-LDH, 2 = MgCr-LDH.

https://doi.org/10.1180/clm.2022.26 Published online by Cambridge University Press

Table 2. Parameters of the pseudo-first and pseudo-second order models.

Sample	Temperature (°C)	Pseudo-first order R^2	Pseudo-first order k_1 (min^{-1})	Pseudo-second order q_e (mmol g^{-1})	Pseudo-second order R^2	Pseudo-second order k_2 (g $mmol^{-1}$ min^{-1})
MgAl-LDH	25	0.9208	0.0041	0.005	0.9973	3.0856
	35	0.9551	0.0047	0.005	0.9978	3.5928
MgCr-LDH	25	0.9206	0.0044	0.004	0.9987	4.4479
	35	0.8351	0.0052	0.004	0.9997	10.0382

with metal–oxygen vibrations are present in hydrotalcite at 650–750 and 800–900 cm^{-1}, and in the spectra of stichtite they are observed at 550–1000 cm^{-1}. The spectral region at <1000 cm^{-1} contains both metal–oxygen vibration bands and bands corresponding to the deformation vibrations of carbonate anions (Kloprogge *et al.*, 2002; Frost & Erickson, 2004; Gunasekaran *et al.*, 2006; Seftel *et al.*, 2008). The two bands in the 950–1100 cm^{-1} range with maxima at 954 and 1076 cm^{-1} recorded for the stichtite sample are due to lizardite and correspond to the stretching vibrations of the SiO_4^{4-} tetrahedra (Hofmeister & Bowey, 2006).

The 'memory effect'

Thermal decomposition and the dehydration–rehydration behaviour (the 'memory effect') were studied in detail for both samples. Complete destruction of the LDH structure and the emergence of oxide phases were detected in both cases at 650°C (Fig. 1c,d). In addition, forsterite and chromite phases were identified for calcined stichtite. In the case of calcined hydrotalcite, calcite can be observed in the XRD trace, as was the case for the original sample. After rehydration, traces of the reconstructed LDH phase were observed for hydrotalcite (Fig. 1e). Reconstruction of the layered structure after the rehydration of stichtite was not observed (Fig. 1f).

Sorption kinetics

The kinetic curves of Congo Red sorption on the natural LDHs are presented in Fig. 6. Sorption on hydrotalcites may involve both surface sorption and exchange between the anions in solution and the anions located in the LDH interlayer. In addition, as with any heterogenous process, sorption is a multistage process and includes diffusion stages that cannot be neglected.

To identify the contribution of each stage to the process, pseudo-first order (Equation 2) and pseudo-second order

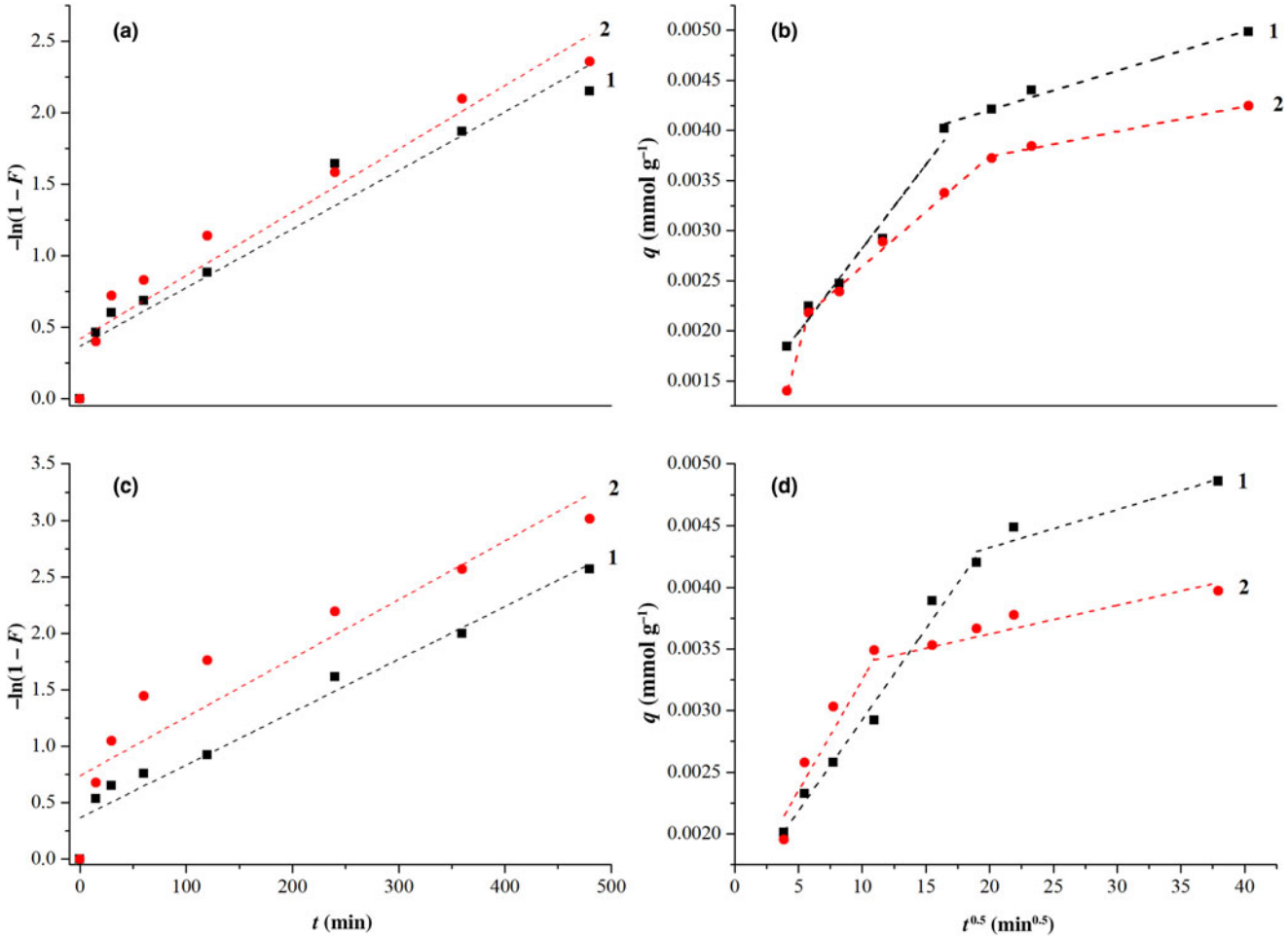

Fig. 8. McKay plots of the kinetic data for the adsorption of Congo Red at (a) 25°C and (c) 35°C. Weber plots of the kinetic data for the adsorption of Congo Red at (b) 25°C and (d) 35°C. 1 = MgAl-LDH, 2 = MgCr-LDH.

https://doi.org/10.1180/clm.2022.26 Published online by Cambridge University Press

(Equation 3) modelling was carried out and the influences of internal diffusion (Equation 4) and external diffusion (Equation 5) were estimated. The kinetic curves obtained using pseudo-first and pseudo-second order models are shown in Fig. 7. The pseudo-first order model does not describe adequately the experimental data for Congo Red sorption on the LDHs. Linear dependence in $\ln(q_e - q_t) = f(t)$ coordinates is observed either at the initial or at the final period of the process. In turn, the pseudo-second order model describes the experimental data sufficiently. In this case, there is linear dependence over the entire investigated time interval. Table 2 demonstrates the parameter values for both models. The rate constant depends significantly on the nature of the LDH. A temperature increase has almost no effect on the rate of sorption on hydrotalcite, whereas the sorption rate on stichtite increases more than twofold under the same conditions.

These results are in accordance with previous work on the sorption of Congo Red on synthetic hydrotalcite (Ayawei *et al.*, 2015). These authors examined the capacity of the zero order kinetic model, second order kinetic model, pseudo-second order kinetic model and third order kinetic model to model their data, and they concluded that the zero order model confirmed the applicability of all of the studied models and so did not allow for any one model to be selected with confidence. It should be taken into account that pure synthetic materials and impure natural minerals consisting of several phases may have varying sorption properties, so the observed differences in the kinetic parameters could perhaps be expected.

The type of diffusion prevailing during sorption is an important characteristic of the process. If external diffusion dominates in the system, the sorbent cannot be considered to be appropriate for large-scale application. To estimate the contribution of external diffusion, the experimental data were processed in terms of diffusion models according to Equations 4 and 5. The rectilinear form of the function $-\ln(1 - F) = f(t)$ is observed only at the initial part of the plot, suggesting that the external diffusion mechanism of adsorption does not describe diffusion adequately; hence, it is necessary to take into account the contribution of intradiffusion (Fig. 8).

Linearity of the plot in the coordinates $q_t = f\left(t^{\frac{1}{2}}\right)$ could serve as evidence that internal diffusion is the limiting stage of the sorption process. However, the experimental plot for the adsorption of

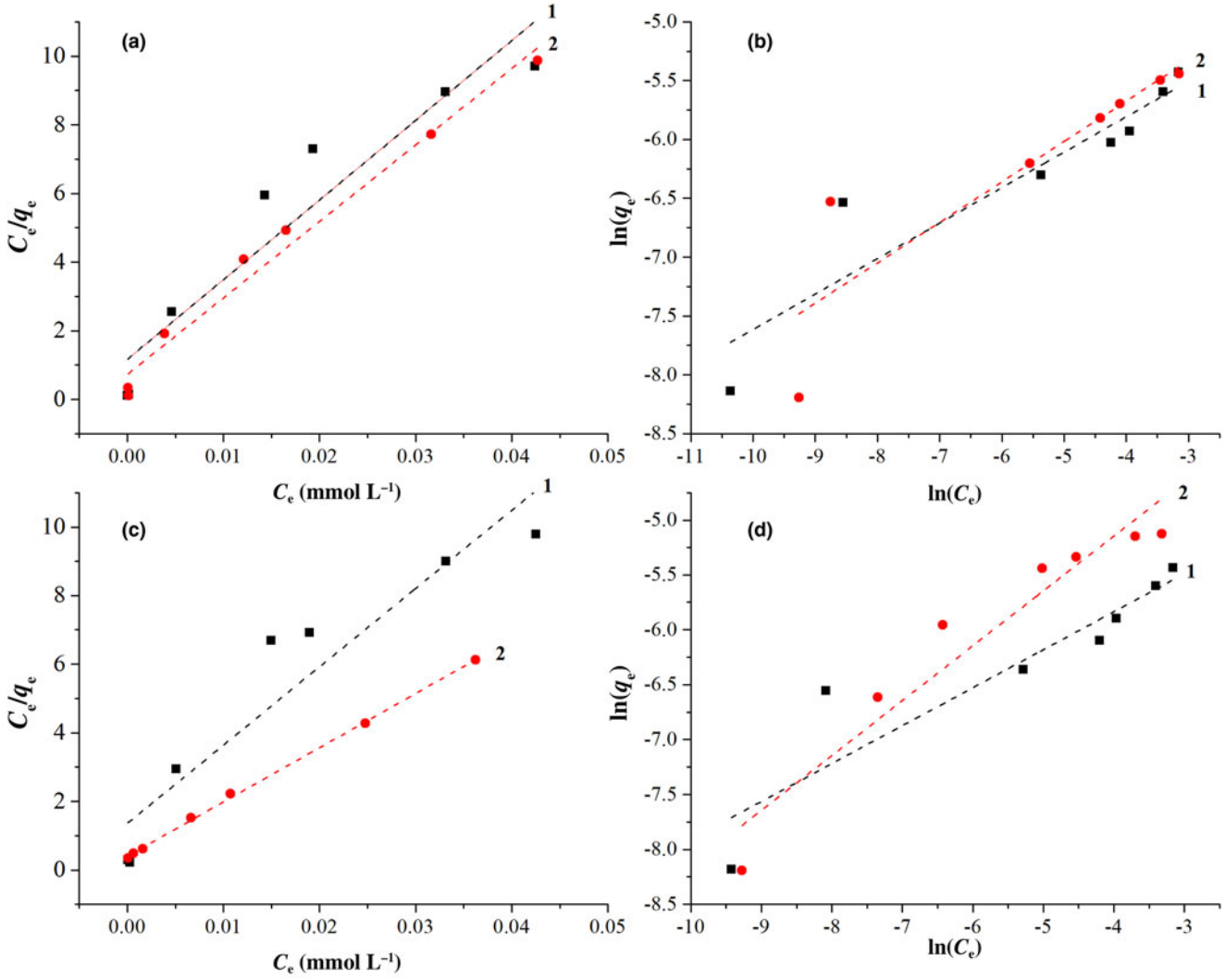

Fig. 9. Linearization of the adsorption isotherms of Congo Red on natural LDH (1 = MgAl-LDH, 2 = MgCr-LDH) on the Langmuir model at (a) 25°C and (c) 35°C and on the Freundlich model at (b) 25°C and (d) 35°C.

https://doi.org/10.1180/clm.2022.26 Published online by Cambridge University Press

Table 3. Sorption parameters for the Langmuir and Freundlich models.

	MgAl-LDH (25°C)	MgAl-LDH (35°C)	MgCr-LDH (25°C)	MgCr-LDH (35°C)
Langmuir model				
R^2	0.8896	0.8777	0.9777	0.9986
q_m (mmol g^{-1})	0.0043	0.0044	0.0045	0.0063
K_L (L $mmol^{-1}$)	199.3	167.9	305.9	391.5
Freundlich model				
R^2	0.9316	0.8193	0.8939	0.9102
n	3.32	2.89	2.91	2.00
K_F	0.0100	0.0116	0.0136	0.0430

Congo Red on natural LDHs is multilinear, and this indicates a mixed diffusion mechanism of sorption.

Thus, the mixed diffusion mode of the process involves several stages. As expected, the first stage of the sorption process is the fastest one. It occurs due to the diffusion of Congo Red ions towards the surface of the LDH. This is followed by a slower stage during which molecules or ions adsorbed on the surface penetrate into the pores of the adsorbent (particle diffusion). The final stage is the dynamic equilibrium adsorption stage (Lei *et al.*, 2017).

Adsorption isotherms

The adsorption isotherms of Congo Red on natural LDHs were used to characterize the sorption capacities of the LDHs. Langmuir and Freundlich models were applied to describe the sorption process (Fig. 9). The sorption parameters for both models, including the calculated values of the maximum adsorption capacity, are listed in Table 3.

The coefficients of determination demonstrate that the sorption on stichtite fit the Langmuir model. However, sorption on hydrotalcite was not modelled adequately, probably due to the presence of significant amounts of impurities with various structures and properties (e.g. calcite). Nevertheless, the maximum sorption capacity values estimated from the Langmuir isotherms for both natural stichtite and hydrotalcite are comparable with the data on Congo Red sorption capacity for the corresponding synthetic LDH (Lafi *et al.*, 2016).

Conclusions

The sorption properties of two natural samples of the hydrotalcite supergroup (hydrotalcite and stichtite) towards the components of an aqueous solution were studied using Congo Red dye as a model sorbate. Both samples consisted mainly of the LDH minerals associated with calcite in the case of hydrotalcite and with lizardite in the case of stichtite. The pseudo-second order kinetic model described the experimental data adequately. In the case of stichtite, temperature had a significant effect on the sorption rate. An increase in temperature of 10°C increased the rate constant by 2.5-fold. Such a temperature dependence was not observed in the case of hydrotalcite. In both cases, the adsorption of Congo Red occurred *via* mixed diffusion. The adsorption isotherm for stichtite was fitted satisfactorily by the Langmuir equation, while for hydrotalcite the correlation was poorer. The minerals studied possess essential characteristics for their use as sorbents. The data obtained could be helpful in the application of natural LDHs for water purification from anionic pollutants.

Financial support. This research was supported by the Russian Foundation for Basic Research, grant no. 18-29-12103.

Competing interests. The authors declare none.

References

Ayawei N., Angaye S.S., Wankasi D. & Dikio E.D. (2015) Synthesis, characterization and application of Mg/Al layered double hydroxide for the degradation of Congo Red in aqueous solution. *Open Journal of Physical Chemistry*, **5**. 58338.

Boid G.E., Adamson A.V. & Maiers L.S. (1949) *Chromatographic Methods of Separation of Ions*. Khimiya, Moscow, Russia [in Russian].

Cavani F., Trifiró F. & Vaccari A. (1991) Hydrotalcite-type anionic clays: preparation, properties and application. *Catalysis Today*, **11**, 173–301.

Chilukoti S. & Thangavel, T. (2019) Enhanced adsorption of Congo Red on microwave synthesized layered Zn–Al double hydroxides and its adsorption behaviour using mixture of dyes from aqueous solution. *Inorganic Chemistry Communications*, **100**, 107–117.

Chubar N., Gilmour R., Gerda V., Mičušík M., Omastova M., Heister K. *et al.* (2017) Layered double hydroxides as the next generation inorganic anion exchangers: synthetic methods *versus* applicability. *Advances in Colloid and Interface Science*, **245**, 62–80.

Correcher V. & Garcia-Guinea J. (2018) Cathodo- and photoluminescence emission of a natural Mg–Cr carbonate layered double hydroxide. *Applied Clay Science*, **161**, 127–131.

Damindarova V.N., Ryl'tsova I.G., Tarasenko E.A., Wang X. & Lebedeva O.E. (2020) Tin-containing layered double hydroxides. *Petroleum Chemistry*, **60**, 444–450.

Daza C.E., Cabrera C.R., Moreno S. & Molina R. (2010) Syngas production from CO_2 reforming of methane using Ce-doped Ni-catalysts obtained from hydrotalcites by reconstruction method. *Applied Catalysis A: General*, **378**, 125–133.

de Castro G.F., Ferreira J.A., Eulálio D., de Souza S.J., Novais S.V., Novais R.F. *et al.* (2018) Layered double hydroxides: matrices for storage and source of boron for plant growth. *Clay Minerals*, **53**, 79–89.

Evans D.G. & Slade R.C.T. (2006) Structural aspects of layered double hydroxides. Pp. 1–87 in *Layered Double Hydroxides. Structure and Bonding*, vol. **119** (X. Duan & D.G. Evans, editors). Springer, Berlin, Germany.

Fan G., Li F., Evans D.G. & Duan X. (2014) Catalytic applications of layered double hydroxides: recent advances and perspectives. *Chemical Society Reviews*, **43**, 7040–7066.

Frost R.L. & Erickson K.L. (2004) Vibrational spectroscopy of stichtite. *Spectrochimica Acta. Part A. Molecular and Biomolecular Spectroscopy*, **60**, 3001–3005.

Goha K.-H., Lima T.-T. & Dong Z. (2008) Application of layered double hydroxides for removal of oxyanions: a review. *Water Research*, **42**, 1343–1368.

Gunasekaran S., Anbalagan G. & Pandi S. (2006) Raman and infrared spectra of carbonates of calcite structure. *Journal of Raman Spectroscopy*, **37**, 892–899.

Ho Y.S. & McKay G. (1999) Pseudo-second order model for sorption processes. *Process Biochemistry*, **34**, 451–465.

Hofmeister A.M. & Bowey J.E. (2006) Quantitative infrared spectra of hydrosilicates and related minerals. *Monthly Notices of the Royal Astronomical Society*, **367**, 577–591.

Kloprogge J.T., Wharton D., Hickey L. & Frost R.L. (2002) Infrared and Raman study of interlayer anions CO_3^{2-}, NO_3^-, SO_4^{2-} and ClO_4^- in Mg/Al-hydrotalcite. *American Mineralogist*, **87**, 623–629.

Krivovichev S.V., Yakovenchuk V.N. & Zhitova E.S. (2012) Natural double layered hydroxides: structure, chemistry, and information storage capacity. Pp. 87–102 in: *Minerals as Advanced Materials II* (S.V. Krivovichev, editor). Springer, Berlin, Germany.

Lafi R., Charradi K., Djebbi M. & Amara A. (2016) Adsorption study of Congo Red dye from aqueous solution to Mg–Al-layered double hydroxide. *Advanced Powder Technology*, **27**, 232–237.

Lagergren S. (1898) About the theory of so-called adsorption of soluble substance. *Kungliga Svenska Vetenskapsakademiens Handlingar*, **21**, 1–39.

Lei C., Zhu X., Zhu B., Jiang C., Le Y. & Yu J. (2017) Superb adsorption capacity of hierarchical calcined Ni/Mg/Al layered double hydroxides for Congo red and Cr(VI) ions. *Journal of Hazardous Materials*, **321**, 801–811.

https://doi.org/10.1180/clm.2022.26 Published online by Cambridge University Press

Li B., Zhang Y., Zhou X., Liu Z., Liu Q. & Li X. (2016) Different dye removal mechanisms between monodispersed and uniform hexagonal thin plate-like MgAl–CO_3^{2-}-LDH and its calcined product in efficient removal of Congo Red from water. *Journal of Alloys and Compounds*, **673**, 265–271.

Liang X., Zang Y., Xu Y., Tan X., Hou W., Wang L. & Sun Y. (2013) Sorption of metal cations on layered double hydroxides. *Colloids and Surfaces A: Physicochemical and Engineering Aspects*, **433**, 122–131.

Liu G., Yang J. & Xu X. (2020) Synthesis of hydrotalcite-type mixed oxide catalysts from waste steel slag for transesterification of glycerol and dimethyl carbonate. *Scientific Reports*, **10**, 10273.

Lopez N.A., Luengo C.V. & Avena M.J. (2019) Uptake/release of vancomycin on/from Mg–Al layered double hydroxides. *Adsorption*, **25**, 1349–1360.

Mantilla A., Tzompantzi F., Fernández A.J.L., Díaz Góngora J.A.I., Mendoza G. & Gómez R. (2009) Photodegradation of 2,4-dichlorophenoxyacetic acid using ZnAlFe layered double hydroxides as photocatalysts. *Catalysis Today*, **148**, 119–123.

Miandad R., Kumar R., Barakat M.A., Basheer C., Aburiazaiza A.S., Nizami A.S. & Rehan M. (2018) Untapped conversion of plastic waste char into carbon–metal LDOs for the adsorption of Congo Red. *Journal of Colloid and Interface Science*, **511**, 402–410.

Mills S.J., Whitfield P.S., Wilson S.A., Woodhouse J.N., Dipple G.M., Raudsepp M. & Francis C.A. (2011) The crystal structure of stichtite, re-examination of barbertonite and the nature of polytypism in MgCr hydrotalcites. *American Mineralogist*, **96**, 179–187.

Mills S.J., Christy A.G., Genin A.G., Kameda T. & Colombo F. (2012) Nomenclature of the hydrotalcite supergroup: natural layered double hydroxides. *Mineralogical Magazine*, **76**, 1289–1336.

Rives V., Arco M. & Martín C. (2014) Intercalation of drugs in layered double hydroxides and their controlled release: a review. *Applied Clay Science*, **88–89**, 239–269.

Seftel E.M., Popovici E., Mertens M., Cool P. & Vansant E.F. (2008) Infrared and Raman spectroscopic study of Sn-containing Zn/Al-layered double hydroxides. *Journal of Optoelectronics and Advanced Materials*, **10**, 3477–3481.

Tanasoi S., Mitran G., Tanchoux N., Cacciaguerra T., Fajula F., Sandulescu I. *et al.* (2011) Transition metal-containing mixed oxides catalysts derived from LDH precursors for short-chain hydrocarbons oxidation. *Applied Catalysis A: General*, **395**, 78–86.

Tezuka S., Chitrakar R., Sonoda A., Ooi K. & Tomida T. (2005) Studies on selective adsorbents for oxo-anions. NO_3^- adsorptive properties of Ni–Fe layered double hydroxide in seawater. *Adsorption*, **11**, 751–755.

Theiss F.L., Ayoko G.A. & Frost R.L. (2013) Stichtite: a review. *Clay Minerals*, **48**, 143–148.

Turvey C.C., Wilson S.A., Hamilton J.L., Tait A.W., McCutcheon J., Beinlich A. & Southam G. (2018) Hydrotalcites and hydrated Mg-carbonates as carbon sinks in serpentinite mineral wastes from the Woodsreef chrysotile mine, New South Wales, Australia: controls on carbonate mineralogy and efficiency of CO_2 air capture in mine tailings. *International Journal of Greenhouse Gas Control*, **79**, 38–60.

Wang Z., Wang E., Gao L. & Xu L. (2005) Synthesis and properties of Mg_2Al layered double hydroxides containing 5-fluorouracil. *Journal of Solid State Chemistry*, **178**, 736–741.

Weber W.J. & Morris J.C. (1963) Kinetics of adsorption on carbon from solution. *Journal of the Sanitary Engineering Division*, **89**, 31–59.

Wei X., Fu Y., Xu L., Li F., Bi B. & Liu, X. (2008) Tungstocobaltate-pillared layered double hydroxides: preparation, characterization, magnetic and catalytic properties. *Journal of Solid State Chemistry*, **181**, 1292–1297.

Zhang H., Chen H., Azat S., Mansurov Z.A., Liu X., Wang J. & Wu R. (2018) Super adsorption capability of rhombic dodecahedral Ca–Al layered double oxides for Congo Red removal. *Journal of Alloys and Compounds*, **768**, 572–581.

Zhitova E.S., Krivovichev S.V., Pekov I. & Greenwell H.C. (2018) Crystal chemistry of natural layered double hydroxides. 5. Single-crystal structure refinement of hydrotalcite, $[Mg_6Al_2(OH)_{16}](CO_3)(H_2O)_4$. *Mineralogical Magazine*, **83**, 269–280.

https://doi.org/10.1180/clm.2022.26 Published online by Cambridge University Press